Thermal Modeling Analysis and Validation of Drilling Manufacturing Process for Aero-Engine Turbine Blades

Chau-Chung Song[1,*], Jian-Hong He[2], and Cheng-Hua Wu[2]

[1]Aeronautical Engineering and Smart Machine and Intelligent Manufacturing Research Center, National Formosa University, Taiwan
[2]Aeronautical Engineering, College of Engineering, National Formosa University, Taiwan
Email: ccsong@nfu.edu.tw (C.-C.S.); 10978110@gm.nfu.edu.tw (J.-H.H.); 10978112@gm.nfu.edu.tw (C.-H.W.)
[*]Corresponding author
Manuscript received October 16, 2023; revised May 25, 2024; accepted July 12, 2024; published August 15, 2024

***Abstract*—Currently, there is a scarcity of research on film-cooling of engine turbine blades, primarily due to the difficulty in accessing technical materials and the high complexity associated with designing curved surfaces. This study employs the heat flow analysis software Simcenter STAR-CCM+ to strategically plan and design the position, angle, and arrangement of heat dissipation holes for the thermal model of engine turbine blade. Subsequently, a simulation analysis is conducted to validate its heat dissipation efficiency. Additionally, experimental verification of the drilling manufacturing process is performed on aero-engine turbine blades. Based on the heat flow simulation results, a drilling model of engine turbine blade is designed for further thermal analysis of cooling efficiency. The drilling position of the workpiece is then transformed and compiled into an electric discharge machining file using the drilling process editing system integrated with the production line. Finally, an automatic production line for the drilling process is constructed to validate the performance and feasibility of the proposed thermal model for aero-engine turbine blades.**

***Keywords*—engine turbine blades, film cooling, thermal model, heat dissipation simulation analysis, drilling process**

I. Introduction

Since 2016, Taiwan has been actively promoting related plans for developing the aerospace industry to expand the supply capacity of Taiwan's aerospace parts manufacturing equipment and continuously optimize the manufacturing technology and process of existing aerospace components to improve industrial efficiency [1–3]. The components required by the aerospace industry have unique requirements and characteristics, such as complex appearance and internal structure, unique materials, and light and thin thickness.

In this paper, we use the heat flow analysis software Simcenter STAR-CCM+ [4, 5] to conduct simulation experiments on the influence of the film hole's jet angle and the film hole's compound angle on the blade's comprehensive cooling efficiency.

II. Theory of Film Cooling

Film cooling is to enter an additional low-temperature flow in the upstream area of the wall surface of the object that needs to be insulated, enter an additional low-temperature flow in the original main flow field and the boundary layer of the wall surface, and form a low-temperature protective layer downstream of the cooling hole to block the high-temperature fluid from direct contact, and reduce the heat transfer to reduce the object. The effect of the surface temperature, and the heat exchange effect between the cooling flow and the main field, gradually increase the temperature of the cooling flow, and the cooling effect is lost [6]. A simplified diagram of film cooling is shown in Fig. 1. According to the position of the blade film hole, it is also divided into various heat dissipation methods, such as impact cooling, film cooling, divergent cooling, etc. The Diagram of the blade heat dissipation method is shown in Fig. 2 [7].

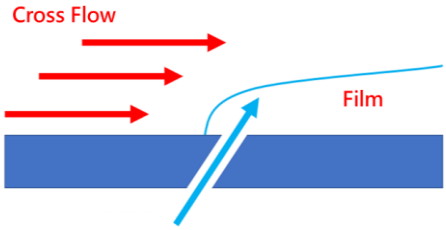

Fig. 1. Diagram of film cooling.

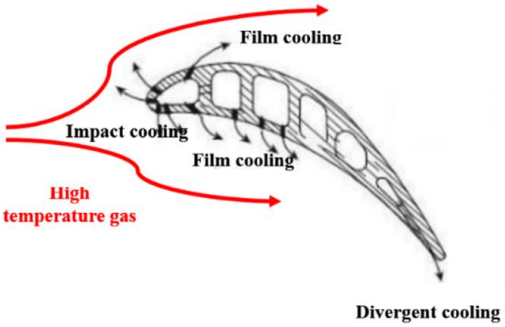

Fig. 2. Diagram of the blade heat dissipation method.

III. Simulation Analysis of Engine Turbine Blade Heat Dissipation

A. Experimental Environment

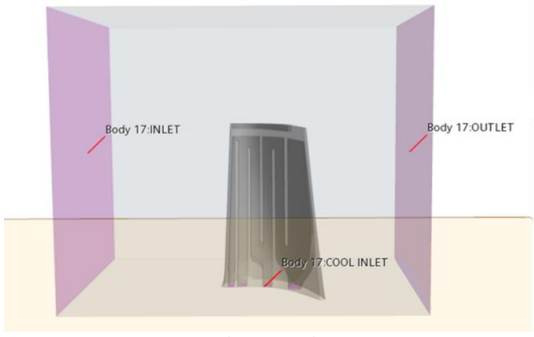

Fig. 3. Model of the heat flow environment.

Fig. 3 is a model of the heat flow environment in this paper. The model's left side is the main inlet, from which high-temperature heat flow is input, and the boundary

condition is set as the velocity inlet. The bottom of the model is the cold flow inlet, which only flows in from the cooling channel inside the blade, and the boundary condition is set as the velocity inlet. The model's right side is the fluid outlet, from which both hot and cold flows flow out, and the boundary condition is set as the pressure outlet. All walls except the blades are treated with an adiabatic wall heat flux boundary condition.

B. Experimental Parameters

There are many parameters affecting the efficiency of film cooling, which can be roughly divided into geometric parameters and flow parameters. Among the geometric parameters, the inclination angle of the film hole greatly influences the cooling efficiency. Among the flow parameters, the blowing ratio M is an important parameter to measure the cooling air volume, which is defined as follows [8]:

$$M = \frac{\rho_c v_c}{\rho_\infty v_\infty} \tag{1}$$

Referring to Eq. (1), ρ is the jet density, ν is the jet velocity, and the subscripts c and ∞ are cold and hot, respectively.

The comprehensive film cooling efficiency η used to evaluate the simulation results is defined as [8]:

$$\eta = \frac{T_g - T_w}{T_g - T_c} \tag{2}$$

Referring to Eq. (2), T_g is the mainstream temperature, T_w is the blade surface temperature, and T_c is the cooling flow temperature. Due to the variable curvature of the blade surface, each block is affected by cooling differently, so T_w is calculated based on the average temperature of the blade surface for comprehensive cooling efficiency.

Table 1 is the parameter setting of fluid, referring to the literature [8], to simulate the high-temperature environment of the actual operation of the turbine engine, and the fluid is an ideal compressible gas. Under the atmospheric pressure of 1atm, the temperature of the main field is 1082.00 K, the velocity is 20.00 m/s, and the turbulence degree is 5.00%. The temperature of the cold flow field is 653.00 K, the blowing ratio M determines the velocity value, the turbulence degree is 5.00%, and the outlet pressure is set to 0.00 Pa.

Table 1. Parameter setting of fluid

Material properties	Heat flow	Cold flow
Entrance velocity	20.00 m/s	Determined by blowing ratio M
Inlet temperature	1082.00 K	653.00 K
Turbulence degree	5.00%	5.00%
Outlet pressure	0.00 Pa	0.00 Pa

The material properties of the heat dissipation blades selected for simulation in this paper are nickel-based alloy Inconel713. This alloy has high creep strength, thermal fatigue, and oxidation resistance and is suitable for making hot-end rotating and static parts working below 900.00 °C. Precision castings, such as turbine working blades, guide vanes, guides, and integral cast turbines, are the most widely used nickel-based superalloy materials in the aerospace industry. Table 2 is the parameter setting table of the solid, and the density is 8000.00 kg/m^3, the thermal conductivity is 20.90 W/m-K, the specific heat is 435.00 J/kg-K, and the initial temperature is 500.00 K.

Table 2. Parameter setting of the solid

Material properties	Solid
Density	8000.00 kg/m^3
Heat conductivity	20.90 W/m-K
Specific Heat	435.00 J/kg-K
Initial temperature	500.00 K

C. Experimental Model Design

Among the various factors that affect film cooling, this thesis chooses the film hole angle and arrangement most relevant to the engine turbine blade drilling process line to conduct heat dissipation simulation. The film hole angle affecting cooling efficiency is divided into the jet and composite angles. Diagram of the jet angle is shown in Fig. 4, which refers to the angle formed by the film hole's axis and the heat flow direction [9]. For the jet angle of the film hole, this paper designs four models of 90°, 75°, 60°, and 45°. The hole spacing is fixed at 2.00 mm, and the size of the film hole is 1 mm in diameter. The model design of the jet hole is shown in Fig. 5.

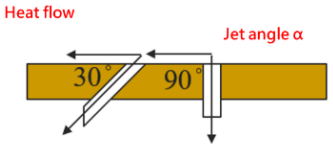

Fig. 4. Diagram of the jet angle.

(a) (b) (c) (d)

Fig. 5. The model design of the jet hole (a) 90°, (b) 75°, (c) 60°, (d) 45°.

Next is the heat dissipation simulation for the compound angle of the film hole. As shown in Fig. 6, the compound angle is formed by the film hole's axis projection on the workpiece's plane and the heat flow direction [10]. In this paper, two angles of 15° and 30° are designed, the hole spacing is fixed at 2.00 mm, and the film hole size is 1.00 mm in diameter. Fig. 7 shows the model design of the compound angle. Due to the changeable curvature of the blade surface, the drilling in some blocks has shown obvious deformation, so it is not easy to increase the compound angle for simulation.

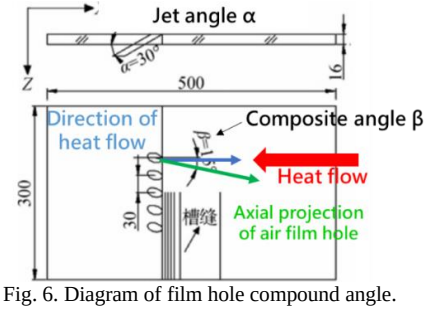

Fig. 6. Diagram of film hole compound angle.

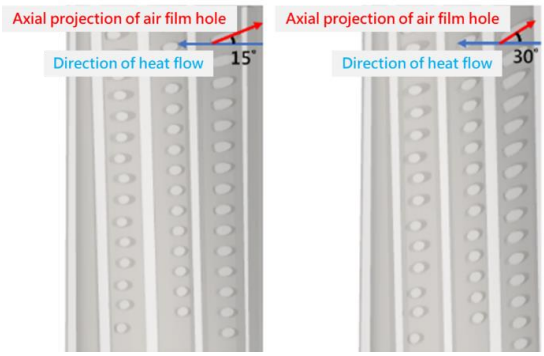

(a) (b)

Fig. 7. Compound angle design (a) 15°, (b) 30°.

IV. Heat Dissipation Simulation Analysis Results

The temperature distribution diagram of the film cooling control group is shown in Fig. 8. This control group has no cooling flow input. Only the main flow and the blades conduct heat exchange. Fig. 9 is the airflow vector diagram of the control group. From Figs. 8 and 9, it can be seen that the temperature of the front end is higher due to the direct impact of the mainstream. Fig. 10 shows the average surface temperature of the control group. The average temperature is 874.926.00 K when the iteration reaches 300.00, and the comprehensive cooling efficiency is 0.48. In the research literature [11], the comprehensive cooling efficiency is about 0.60~0.80, so the cooling efficiency of the control group is inferior.

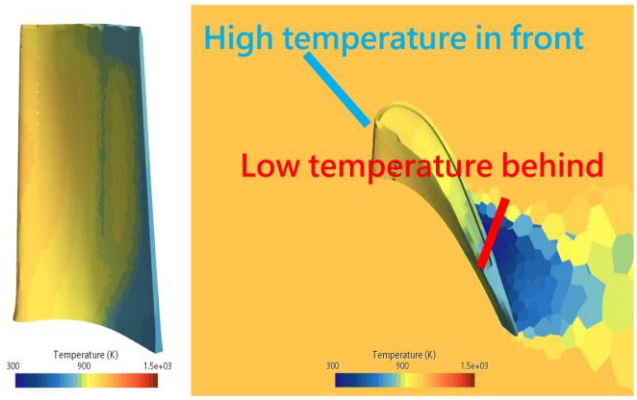

Fig. 8. Temperature distribution diagram of the film cooling control group.

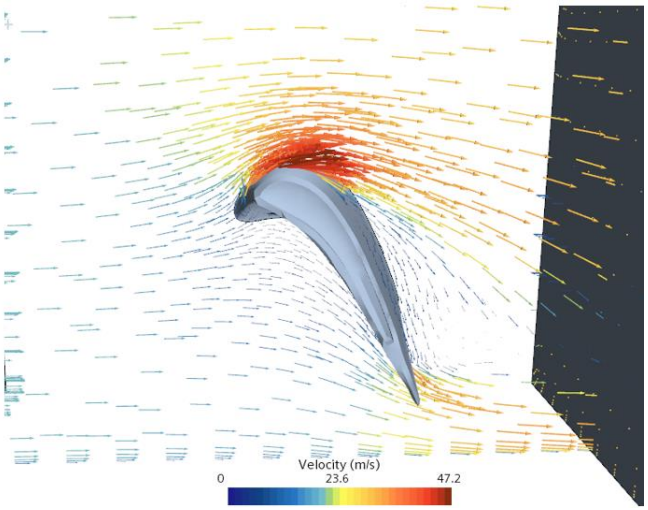

Fig. 9. Airflow vector diagram of film cooling control group.

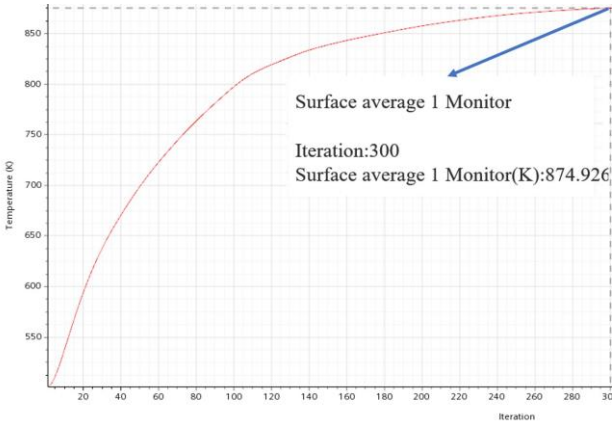

Fig. 10. Average surface temperature of film cooling control group.

A. Jet Angle Simulation Results

From the simulation results of jet angles of 90°, 75°, 60°, and 45°, it can be concluded that the cooling range increases with the change of jet angle, and among these four angles, the jet angle is 45°, as shown in Fig. 11. The cooling area caused by the surface is the largest. On the simulated blade model, it can be seen that the temperature in some areas is higher. The reason mentioned in [12] is that the temperature field near the blade's leading edge is higher because the leading edge film hole flow is insufficient and is directly washed by the main flow. However, due to the contraction and expansion of the cold air channel near the trailing edge, an enormous vortex will be generated at the entrance to affect the internal heat transfer, resulting in a high-temperature area at the trailing edge. The local low temperature at the end of the blade is due to the increase in the flow of cold air due to the cold air discharged from the film hole passing through the elbow and then flowing to the end of the blade. Fig. 12 is the temperature distribution of the pressure surface of the turbine blade taken by the infrared thermal imager. It can be seen from the airflow vector diagrams of the film holes with jet angles of 90°, 75°, 60°, and 45° that the film holes with jet angles of 90°, as shown in Fig. 13(a), the Airflow is only discharged from the film holes, not in the surface of the blade flows to form a film, so the cooling efficiency is the worst, and the cooling range does not change much. With the change of the jet angle, the Airflow is gradually attached to the blade, and the cooling flow also increases. At 45°, as shown in Fig. 13(b), the Airflow is the largest, the cooling efficiency is the best, and the cooling range is the largest.

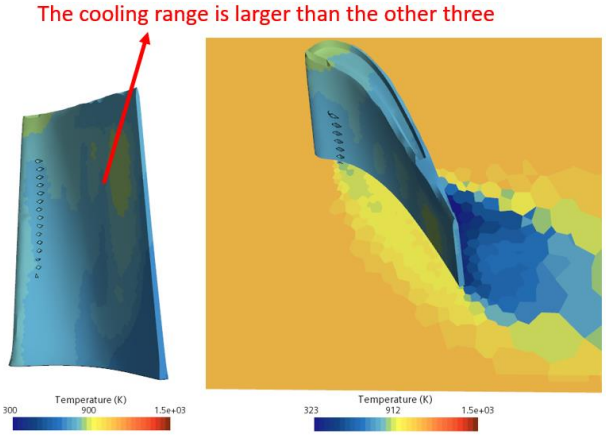

Fig. 11. Temperature diagram of film hole with jet angle of 45°.

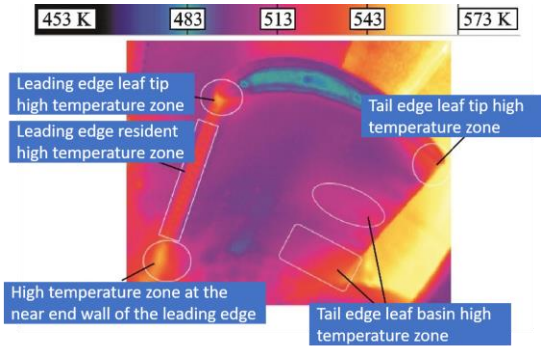

Fig. 12. Temperature distribution diagram of turbine blade pressure surface.

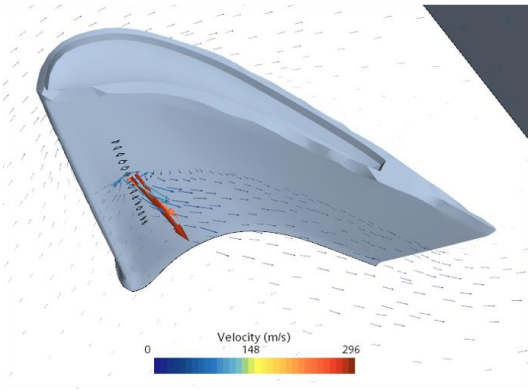

(a)

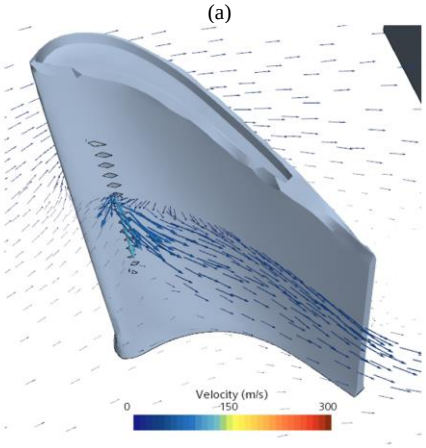

(b)

Fig. 13. Airflow vector diagram of film hole with the jet angle of (a) 90°, (b) 45°.

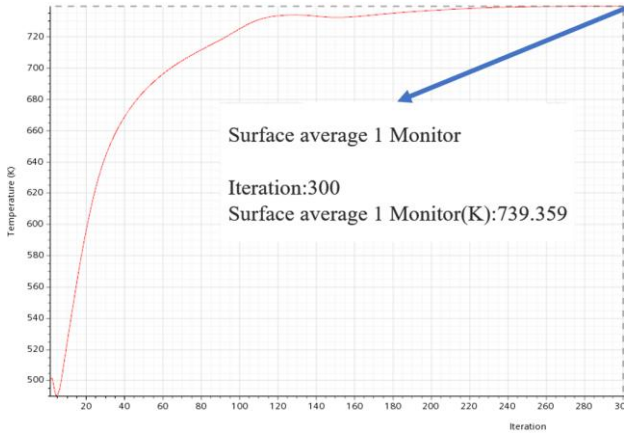

Fig. 14. Average surface temperature of the film hole at a jet angle of 45°.

While the iteration reaches 300.00, the average surface temperatures of the film holes with jet angles of 90°, 75°, 60°, and 45° are 773.18 K, 762.15 K, 760.08 K, and 739.36 K, respectively, and the comprehensive cooling efficiency is 0.72, 0.75, 0.75, and 0.80. Since the jet angle of 45° has the most extensive cooling range, it has the effect of cooling most of the blade surface. As shown in Fig. 14, the cooling efficiency of the average surface temperature of the film hole at a jet angle of 45° is the best among the four angles.

B. Results of Compound Angle Simulation

Fig. 15 is the temperature distribution diagrams of the film holes with compound angles of 15° and 30°, respectively; those figures show that the compound angle has an apparent cooling effect on the upper edge of the blade tail end and the cooling efficiency of other areas is not as good as that of no degradation due to compound angles.

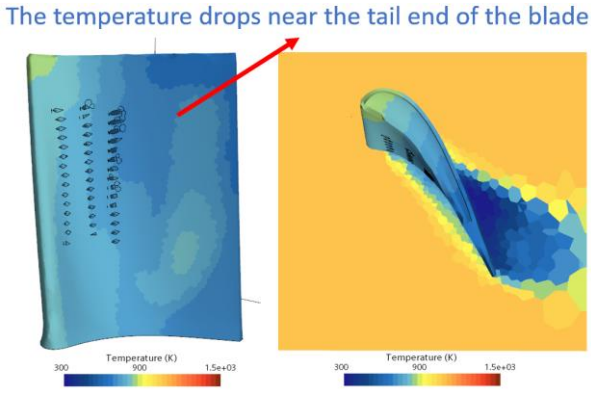

(a)

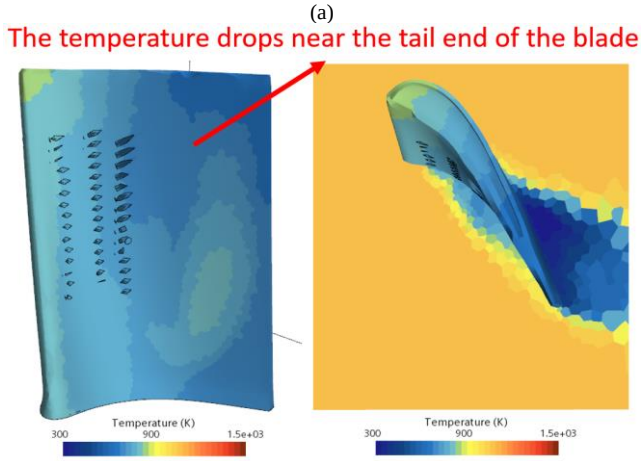

(b)

Fig. 15. Temperature distribution diagram of film hole with the composite angle of (a) 15°, (b) 30°.

Fig. 16 is the airflow vector diagrams of film holes with compound angles of 15° and 30°, respectively, and the Airflow is higher than that of film holes without compound angles. Through the internal perspective view of Figs. 17 and 18, it can be seen that the Airflow inside the channel without compound angle film holes is irregular, while the Airflow inside the channel with compound angle film holes flows neatly and is guided by the film holes, so Airflow with composite keratin film holes will be higher than without composite keratin film holes.

Fig. 19 is the average surface temperature diagrams of the 15° and 30° compound angle film holes, respectively. When the iteration reaches 300.00, the average surface temperature is 715.02 K and 716.73 K, and the comprehensive cooling efficiency is 0.86 and 0.85, respectively, consistent with the simulation results without a compound angle. The resulting overall cooling efficiency is an increase compared to 0.84. Since the compound angle increases the coverage area of the cold air film by deflecting the airflow direction, it achieves

better cooling efficiency, but the increase in the compound angle does not increase the coverage area, so the cooling efficiency difference between the two is not significant.

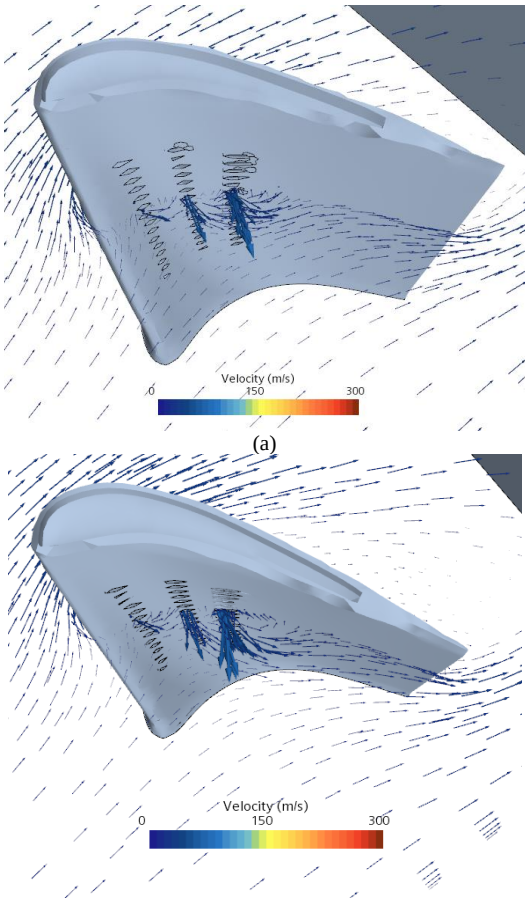

Fig. 16. Airflow vector diagram of film hole with the composite angle of (a) 15°, (b) 30°.

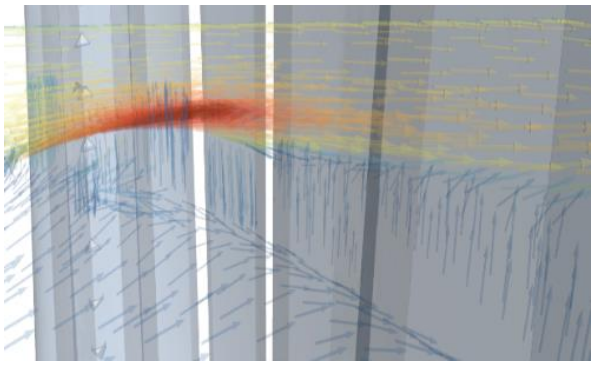

Fig. 17. Perspective view of airflow without composite corner film holes.

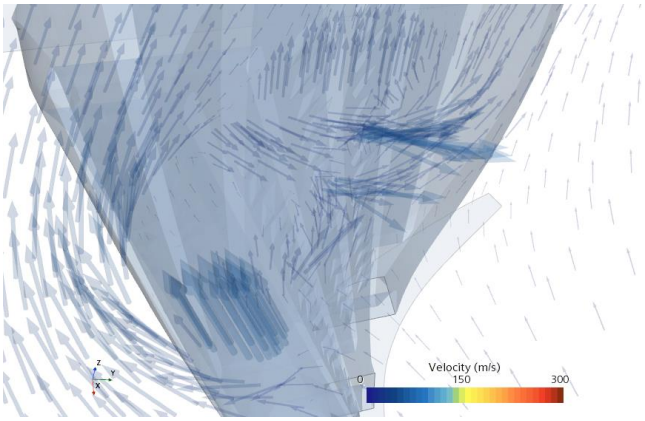

Fig. 18. Airflow perspective view of compound angle 30° membrane hole.

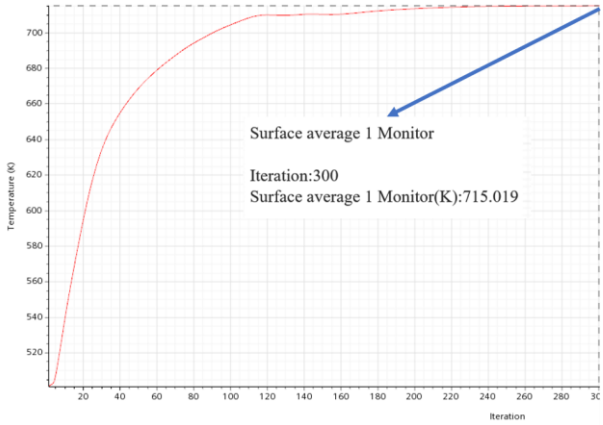

Fig. 19. Average surface temperature diagram of the film hole at a compound angle of (a) 15°, (b) 30°.

V. Experimental Results

Based on the heat flow simulation results in the previous section, this paper designs and plans the drilling workpiece and uses STAR-CCM+ heat flow analysis software to simulate and analyze its cooling efficiency. According to the data obtained from the simulation results, the cooling efficiency of a jet angle of 45° is the highest but limited by the angle between the electrode and the blade of the Electronic Document Management (EDM) in this production line, it is difficult to drill with a jet angle of 45°, and the final film hole The jet angle is designed with 60°. Since the cooling efficiency of the compound angle of 15° and 30° is not much different, and the shape of the drilling designed with the compound angle of 15° is less deformed, the compound angle of the film hole is selected to be designed at 15°. Fig. 20 is the design drawing of the drilling workpiece.

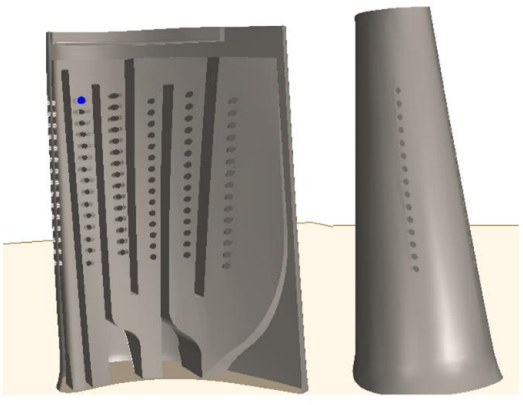

Fig. 20. Design drawing of blade drilling.

Figs. 21 and 22 are the temperature distribution diagrams of the drilling workpiece. Except that there is no cooling channel and film coating at the upper end of the blade's leading edge for cooling and heat dissipation, the temperature distribution of the other blocks has been improved. In the picture, it can be seen that there is a complete cold flow on the outer layer of the film hole to cover the blade and form a film. Fig. 23 is the airflow vector diagram of the drilling workpiece, it can be seen that the film holes on the side have a slight impact on the mainstream, reducing the impact of the mainstream on the back of the blade, increasing the cooling range of the blade, and achieving the purpose of cooling.

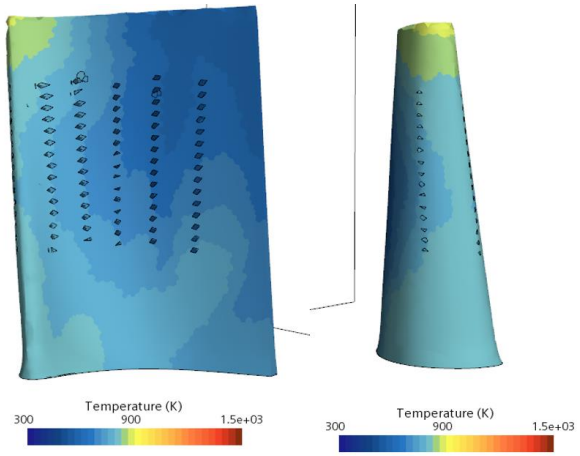

Fig. 21. Temperature distribution diagrams of the drilling workpiece.

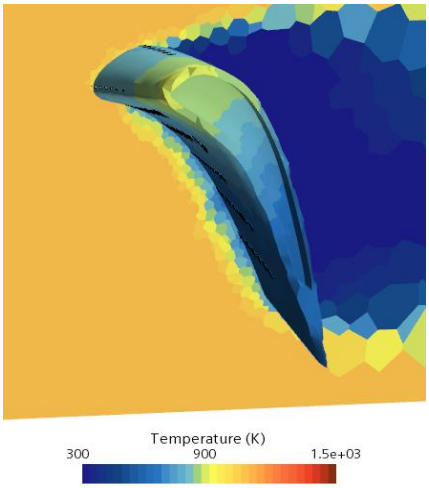

Fig. 22. Temperature nephogram of drilling workpiece.

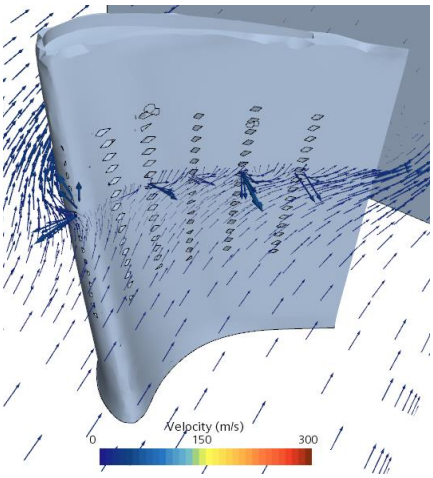

Fig. 23. Airflow vector diagram of drilling workpiece.

Fig. 24 is the average surface temperature diagram of the drilling workpiece. When the iteration reaches 300.00, the average surface temperature is 698.28 K, and the comprehensive cooling efficiency is 0.89. Compared with the comprehensive cooling efficiency of the control group in the simulation experiment of 0.48, it is 1.86 times higher. Compared with the comprehensive cooling efficiency of 0.60~0.80 obtained in the research experiments of other works of literature, the cooling efficiency is also improved by 1.1 times.

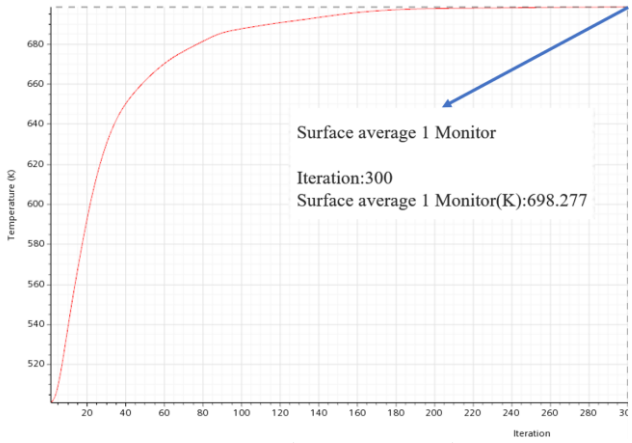

Fig. 24. The average surface temperature of the blade.

After the simulation is completed to confirm the cooling efficiency of the drilling workpiece, the drilling process editing system integrated with the engine turbine blade drilling process production line can convert and compile the model drilling coordinates into a processing file for processing, then the operation of drilling machining. Figs. 25 and 26 are the operation diagrams of the process editing system. Import the machining point coordinates into the editing system and perform automatic conversion and compilation to generate EDM files, then transmit the EDM file to the EDM machine and start the EDM production line for fully automated processing. The robotic arm will place the workpiece to be processed on the jig inside the EDM. The operation of the robot arm is shown in Fig. 27.

After the mechanical arm retracts to the standby point, the valve of the EDM machine will be closed, and the EDM operation will start. The operation of EDM is shown in Fig. 28. After the electrical discharge machining, and the mechanical arm takes out the finished product, which is placed at a fixed point to complete the entire processing process.

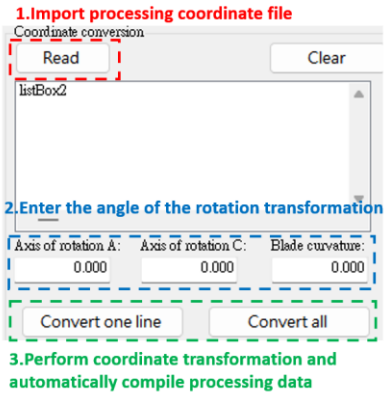

Fig. 25. Machining coordinate conversion.

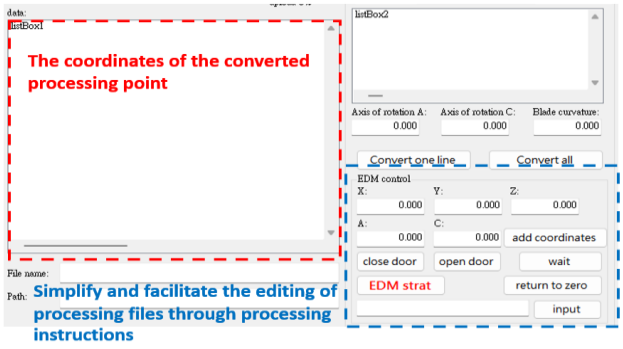

Fig. 26. Coordinate transformation completed and machining instruction edited.

Fig. 27. The operation of the robot arm.

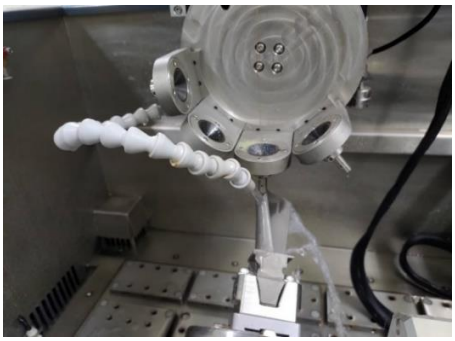

Fig. 28. The operation of EDM.

Frontal comparison of the workpiece after processing is shown in Fig. 29. Since the blade's surface is curved, it is easy to touch the electrode of the electric discharge machine. To avoid touching the blade's surface, the electrode cannot be close to the processing target point, and finally, the copper tube of the electrode is extended too long to reduce the machining accuracy. Significantly reduced, so the first row of processing is not ideal. The side view of the workpiece after processing is shown in Fig. 30. Since the machining of the side row is least affected by the curvature of the blade surface, the error of machining coordinates transformation, and the error of machining accuracy are the least affected, so the machining situation is the most ideal.

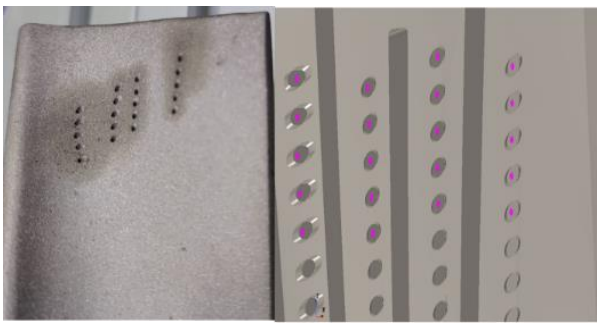

Fig. 29. Frontal comparison of the workpiece after processing.

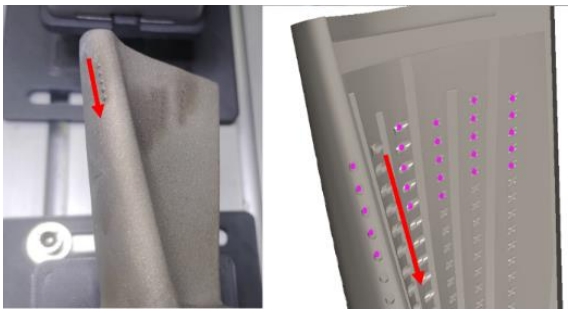

Fig. 30. Side view of workpiece after processing.

VI. Conclusion

In this paper, we use the heat flow analysis software Simcenter STAR-CCM+ to conduct simulation experiments on the influence of the film hole's jet angle and the film hole's compound angle on the blade's comprehensive cooling efficiency. According to the simulation results, the following conclusions can be drawn: First, in the film holes with jet angles of 90°, 75°, 60°, and 45°, jet angle 45° has the largest covered area and cooling efficiency. Second, the Airflow of the film holes at jet angles of 75°, 60°, and 45° is gradually attached to the blade, cooling flow rate, cooling efficiency, and covered area also increase and reach the maximum at 45°. Third, the internal perspective view shows irregular airflow inside the channel without compound angle film holes. In contrast, the internal airflow in the track with compound angle film holes flows neatly and is guided by the film holes, so there is a compound angle. Film holes have higher airflow and cooling efficiency than those without compound angles. In addition, the drilling process editing system we developed is integrated with the engine turbine blade drilling process production line, the drilling coordinate conversion is compiled into an EDM file, and the drilling machining action is performed. It can be seen from the front comparison picture of the finished product that the electrode of the electric discharge machine is easy to touch due to the curvature of the blade surface. To avoid touching the blade surface, the electrode cannot be close to the processing target point, and finally, the copper tube of the electrode is extended too long to reduce the machining accuracy. Therefore, it is necessary to pay attention to the limit of the precise penetration angle of the electric discharge machine before designing the penetration angle.

Conflict of Interest

The authors declare no conflict of interest.

Author Contributions

Chau-Chung Song is the lead of this research plan and manages the financial resources. Jian-Hong He is responsible for performing the system modeling and simulation analysis for this paper. Cheng-Hua Wu is responsible for the development and execution of system software. Jian-Hong He and Cheng-Hua Wu are responsible for the establishment of the automated production line and the validation of processing experiments. All authors approve the final version.

FUNDING

This research is supported by the National Science and Technology Council, Taiwan, R.O.C. under Grant: MOST 109-2218-E-150-002, 110-2622-E-150-010, and MOST 110-2221-E-150-041.

REFERENCES

[1] Administration Department. The development plan of Productivity 4.0. Taiwan Economic Forum. [Online]. 13(3). Available: https://reurl.cc/70686d

[2] W. N. Zhan. The impact and opportunities of Industry 4.0 on Taiwan's industries. Industrial Development Bureau, Ministry of Economic Affairs. [Online]. Available: https://reurl.cc/QR8q1p

[3] M. J. Wu. Productivity 4.0 promotion strategy and future prospects. Industrial Development Bureau, Ministry of Economic Affairs. [Online]. Available: https://reurl.cc/r9Nqzk

[4] Megaflow Technology Co., Ltd. (2020). Simcenter STAR-CCM+ CFD multi-physics coupling analysis platform. [Online]. Available: https://megaflow.com.tw/simcenter-star-ccm/?gclid=CjwKCAjwtIaVBhBkEiwAsr7-c7MWMcX9gqkJ65LphOrTwP6HGSLNxUUk_b0PIXs903ZW6kCCgwGoGRoCMHsQAvD_BwE (in Chinese)

[5] Siemens Digital Industries Software. (2022). Computational Fluid Dynamics (CFD) Simulation. [Online]. Available: https://www.plm.automation.siemens.com/global/en/products/simulation-test/fluid-dynamics-simulation.html

[6] Y. K. Liao, "A study of effects of a moving blade on film-cooling process," Master's thesis, Department of Mechanical Engineering, National Chiao Tung University, 2006.

[7] CAESES in the parametric modeling application of turbine cooling blades (November 13, 2019). [Online]. Available: http://www.cfluid.com/forum.php?mod=viewthread&tid=213168 (in Chinese)

[8] R. F. Wang, H. K. Bao, and Y. He, "Correction of empirical formula for gas film cooling efficiency based on numerical simulation," *Mechanics Research*, vol. 9, no. 2, pp. 32–47, 2020.

[9] L. F. Liu, R. L. Dong, H. H. Shi, W. J. Shen, W. Chen, and K. Xie, "Experimental research on film cooling of different compound angles based on infrared thermography technology," *Journal of Zhejiang Sci-Tech University (Natural Science Edition)*, vol. 33, no. 4, 2015. (in Chinese)

[10] K. Xie, R. L. Dong, H. H. Shi, W. J. Shen, and W. Chen, "Experimental investigations of influence of compound angle and arrangement modern flat air film cooling effect," *Journal of Zhejiang Sci-Tech University (Natural Sciences)*, vol. 30, no. 4, 2017. (in Chinese)

[11] J. T. Wei, B. Zhong, Y. P. Liu *et al*., "Experimental investigation on integrated cooling characteristics of air cooled TurbineBlade," *Journal of Chongqing University of Technology (NaturalScience)*, vol. 35, no. 9, pp. 278–286, 2021. (in Chinese)

[12] L. C. Deng, W. T. Xuan, B. Zhong *et al*., "Experimental research on surface temperature field and comprehensive cooling effect of turbine blade," *Journal of Nanjing University of Aeronautics & Astronautics*, vol. 53, no. 3, pp. 442–448, 2021.